

# Demonstration of Advanced Timing Schemes in Time-Resolved X-ray Diffraction Measurements

Daniel Schmidt,<sup>†</sup> David. v. Stetten,<sup>‡</sup> Michael Agthe,<sup>‡</sup> Arwen R. Pearson,<sup>¶</sup>  
Goddfrey .S. Beddard,<sup>§</sup> Briony A. Yorke,<sup>||</sup> Friedjof Tellkamp,<sup>⊥</sup> and Peter  
Gaal<sup>\*, #, †</sup>

<sup>†</sup>*TXproducts UG (haftungsbeschränkt), Luruper Hauptstr. 1, 22547 Hamburg, Germany*

<sup>‡</sup>*European Molecular Biology Laboratory (EMBL), Notkestrasse 85, 22607 Hamburg,  
Germany*

<sup>¶</sup>*University of Hamburg, Luruper Chaussee 149, 22761 Hamburg, Germany*

<sup>§</sup>*School of Chemistry, University of Edinburgh, David Brewster Road, EH9 3FJ, UK*

<sup>||</sup>*School of Chemistry, University of Leeds, Leeds, UK*

<sup>⊥</sup>*Max Planck Institute for the Structure and Dynamics of Matter, Luruper Chaussee 149,  
22761 Hamburg, Germany*

<sup>#</sup>*Leibniz-Institut für Kristallzüchtung, Max-Born-Str. 2, 12489 Berlin, Germany*

E-mail: peter.gaal@ikz-berlin.de

## abstract

We present time-resolved X-ray diffraction measurements using advanced timing schemes that provide high temporal resolution while also maintaining a high flux in the X-ray probe beam. The method employs patterned probe pulse sequences that are generated with the *WaveGate* solid-state pulse picker. We demonstrate the feasibility of our method at two different beamlines on millisecond and microsecond timescales.

## Introduction

Next-generation synchrotrons<sup>1</sup> present exciting opportunities for researchers across various fields, including biology, chemistry, life sciences, materials science, and engineering.<sup>2</sup> A key advantage of these new sources is their improved ability to observe samples *in situ* within their natural environments and monitor their dynamics *in operando*. The relevant timescales for detecting structural dynamics typically range from picoseconds to microseconds. Such experiments are almost exclusively conducted using pump-probe schemes where a short stimulus, such as a laser pulse, excites the sample, and a subsequent probe pulse detects the transient state at a specific pump-probe delay. The temporal resolution of this scheme is generally limited by the duration of the probe pulse, typically around 100 ps at a synchrotron source.<sup>3,4</sup> Using only one synchrotron pulse per excitation cycle ensures the best achievable time resolution but also reduces the photon flux because all other pulses within the excitation cycle are ignored. However, sample and measurement equipment are still exposed to the X-ray beam throughout the whole excitation cycle, which may cause saturation effects or even damage to the sample or to the measurement equipment.<sup>5</sup> Thus, when using the pump-probe method, researchers face a trade-off between temporal resolution and the sensitivity of their experiments.

In this article, we discuss advanced timing schemes that overcome these limitations. Specifically, we present a method that employs patterned probe sequences derived from a Hadamard transform. The Hadamard transform is already applied in spectroscopy<sup>6,7</sup> and microscopy<sup>8,9</sup> to maintain spectral or spatial resolution while increasing a measurement's sensitivity.<sup>10-12</sup> Researchers have already adapted it in the time domain successfully by imaging a rotating disc with an X-ray beam.<sup>5,13</sup> These results demonstrate the potential to significantly improve time-resolution, however, Hadamard time-domain measurements are not commonly performed due to the lack of flexibility in patterning the time structure of the X-ray beam. We employ a solid-state pulse picker (*WaveGate*, TXproducts) to overcome this constraint.

# Employing a Hadamard Transform for Time-Domain Measurements

In this section we will briefly describe the working principle of the Hadamard transform specifically in the context of time-domain measurements. Consider the standard time-resolved measurement approach, *i.e.*, the pump-probe method. Let  $t$  denote the pump-probe delay axis. The pump-probe measurement divides this axis in  $n$  discrete time windows called delays  $t_n$ . For simplicity, assume that all  $t_n$  have the same duration  $\delta t_n$  although this is not a necessary condition. In the pump-probe scheme, each time window is filled with a probe pulse and a measurement, *e.g.*, a detector image  $W$  is recorded for each delay. Thus, the full dataset contains  $W_n$  measurements or detector images which represent the transient response  $R(t_n) = R_n$  of the sample. Figure 1 a) depicts the pump-probe scheme in a simple scenario where the delay axis  $t$  is split into  $n = 3$  time windows. Each column in Figure 1 a) depicts a probe sequence, which in turn contains only one probe pulse. This means that only one time window in the probe sequence is filled. The probe sequences are represented by the following delay or **M**-matrix:

$$\mathbf{M} = \begin{bmatrix} 1 & 0 & 0 \\ 0 & 1 & 0 \\ 0 & 0 & 1 \end{bmatrix} \quad (1)$$

The measurement matrix (which is an identity or unit matrix) represents the time-points in a traditional pump-probe experiment but we don't tend to actively consider this fact in a pump-probe experiment. For the sake of demonstration, each detector image is obtained by multiplying the **M**-matrix with the transient sample response **R**, *i.e.*,  $\mathbf{W}_n = \mathbf{M}_{n,:} \times \mathbf{R}$  ( $S_{n,:}$  denotes the  $n$ -th row of the **M**-matrix). In reality, we obtain the detector images from measurements and use them to calculate the transient sample response. This is equivalent to the inverse operation  $\mathbf{R} = \mathbf{M}^{-1} \times \mathbf{M}$ . Due to the symmetry of **M** the inverse operation is simple because  $\mathbf{M} = \mathbf{M}^{-1}$ .

Consider now a different scheme for time-resolved measurement that employs probe sequences with more than one time window filled. The scheme is sketched in Figure 1 b). Intuitively, it may seem that this measurement cannot yield the same temporal resolution as the previously described pump-probe method. This is however not the case.

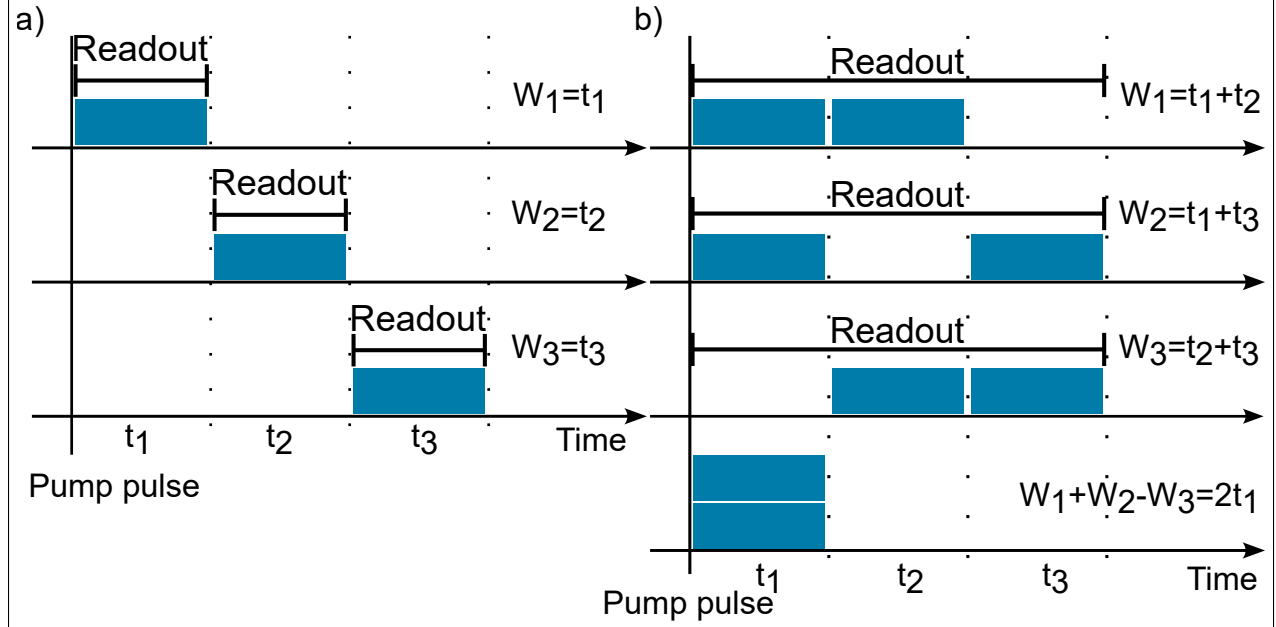


Figure 1: **Time-resolved measurement schemes:** a) Pump-probe method: the delay axis is divided into time windows which are filled with probe pulses in consecutive measurements. Each measurement captures the transient state at one delay. b) Hadamard method: multiple windows on the delay axis are filled with probe pulses. The transient state at each delay (only delay  $t_1$  is shown) can be retrieved during post processing using all measurements.

To demonstrate this, we define a  $\mathbf{S}$ -matrix which contains the probe sequences. Again, we choose a simple example with  $n = 3$  time windows. The  $\mathbf{S}$ -matrix is derived from a Hadamard matrix<sup>14–16</sup> and has the form

$$\mathbf{S} = \begin{bmatrix} 1 & 1 & 0 \\ 1 & 0 & 1 \\ 0 & 1 & 1 \end{bmatrix} \quad (2)$$

The first measurement yields  $\mathbf{S}_1 = \mathbf{S}_{1,:} \times \mathbf{R} = (1 \cdot \mathbf{R}_1) + (1 \cdot \mathbf{R}_2) + (0 \cdot \mathbf{R}_3)$ , *i.e.*, it is a summation over a total of two probe pulses in windows 1 and 2. Again, we want to obtain

the sample response  $R$ , thus we perform the inverse operation  $\mathbf{R} = \mathbf{S}^{-1} \times \mathbf{W}$ , where

$$\mathbf{S}^{-1} = 0.5 \cdot \begin{bmatrix} 1 & 1 & -1 \\ 1 & -1 & 1 \\ -1 & 1 & 1 \end{bmatrix} \quad (3)$$

For the first time window of the transient response we find  $\mathbf{R}_1 = \mathbf{S}_{1,:}^{-1} \times \mathbf{W} = (0.5 \cdot \mathbf{W}_1) + (0.5 \cdot \mathbf{W}_2) - (0.5 \cdot \mathbf{W}_3)$ . It is immediately evident that full measurement of all probe sequences is necessary to retrieve the transient state  $\mathbf{R}_1$ . The same is true for any other transient state at any other delay. Figure 1 b) depicts graphically how the first delay point can be retrieved.

To conclude this section, we want to point out the following general remarks on time-domain Hadamard measurements: First, the Hadamard method can provide the same time resolution as the pump-probe method. Second, to retrieve the time-resolved response in a measurement one must first measure a full dataset of probe sequences and extract the dynamic response through the inverse operation  $\mathbf{R} = \mathbf{S}^{-1} \times \mathbf{W}$ .

The advantage of the Hadamard method is the increased sensitivity and resolution, in this case along a temporal axis. Specifically, it allows the probing of fast processes with intense probe pulses that encompass multiple delay windows. A necessary requirement for using the Hadamard method is the ability to generate the complex probe sequences. We will present a solution to this challenge in the following section.

## Generating Hadamard Sequences in the Time Domain

Advanced timing schemes like the one discussed in the previous section are not commonly used in x-ray science. The reason is the lack of methods to easily modulate the time structure of synchrotron beams to deliver the complex, irregular Hadamard time sequences. We have recently presented a full characterization of a programmable solid state pulse picker that can achieve exactly this.<sup>17</sup> The device is called *WaveGate*. Here, we will only briefly introduce

its working principle and list the main performance parameters.

The *WaveGate* consists of two crystalline piezoelectric substrates that are mounted in a double monochromator configuration, as shown in Figure 2 a). The first crystal is the so-called active crystal, a surface view is depicted in Figure 2 b). The interdigitated transducer (IDT) at the top is connected to an external harmonic signal generator with a frequency resonant to the IDT's eigenfrequency. The piezoelectric effect converts the time-dependent electric field of this signal into a time-dependent, periodic pressure wave which propagates as a surface acoustic wave (SAW) along the surface of the crystal. When the SAW overlaps with an impinging x-ray beam, it acts as a grating, diffracting the x-ray beam into artificial satellites of a structural Bragg reflex of the piezoelectric substrate. The diffraction efficiency of these satellites can reach 30% or more of the incident beam. The on-off switching time can be as short as 100 ns and the suppression of photons in the off-state is better than  $10^{-4}$ . A detailed explanation of the functionality and specification of the *WaveGate* is presented elsewhere.<sup>17</sup>

An exemplary Hadamard sequence generated by the *WaveGate* with  $n=7$  time windows is plotted in Figure 2 c). Note that, in this example, the duration  $\delta t_n$  of the time windows  $n$  is variable, *i.e.*, the duration of  $t_0 = 0$  is  $\delta t_0 = 700$  ns and the duration  $\delta t_6$  is 10  $\mu$ s. Each time window is separated from its adjacent window by vertical dashed lines. The full Hadamard sequence reads 1010011. To modulate the time-dependent transmission of the x-ray beam through the *WaveGate*, we trigger the *WaveGate* signal generator with the same sequence and modulate each element  $n$  with its appropriate duration  $\delta t_n$ . The active trigger generates an output at the signal generator which translates into diffraction satellites as previously described. We provide TANGO<sup>18</sup> and EPICS<sup>19</sup> servers to incorporate the necessary hardware into BLISS<sup>20</sup> or BlueSky<sup>21</sup> or similar beamline control environments.

Figure 2 a) shows a schematic of the *WaveGate* installed in a beamline. The experiments presented in the next section were performed at beamlines P14(EH2-T-REXX)<sup>22</sup> and P23 at PETRA III, DESY. We used a bunchmarker signal to synchronize the *WaveGate* to

the bunches in the storage ring. However, for time windows much larger than the bunch separation, the synchronization can be omitted. In this case, the *WaveGate* delivers a trigger signal to synchronize the rest of the experiment to the Hadamard time sequence.

## Monitoring Mechanical Motion with Hadamard Time Domain Measurements

In the following we demonstrate the ability to resolve transient dynamics using the advanced timing scheme discussed in the previous sections. We performed two measurements to exemplify the method: first, we monitor the back-and-forth motion along the x-ray beam axis of a translation stage using Debye-Scherrer diffraction from a powder sample and second, we monitor the micromechanical oscillation of a 500 nm thin SiN membrane after absorption of a laser pulse by Laue diffraction.

In both cases we employ a  $7 \times 7$  **S**-matrix that is displayed in Equation 4.

$$\mathbf{S}_7 = \begin{bmatrix} 1 & 1 & 1 & 0 & 1 & 0 & 0 \\ 1 & 1 & 0 & 1 & 0 & 0 & 1 \\ 1 & 0 & 1 & 0 & 0 & 1 & 1 \\ 0 & 1 & 0 & 0 & 1 & 1 & 1 \\ 1 & 0 & 0 & 1 & 1 & 1 & 0 \\ 0 & 0 & 1 & 1 & 1 & 0 & 1 \\ 0 & 1 & 1 & 1 & 0 & 1 & 0 \end{bmatrix} \quad (4)$$

For completeness, the inverse matrix  $\mathbf{S}^{-1}$  is generated by Equation 5.<sup>11</sup>

$$\mathbf{S}^{-1} = 2 \left( 2\mathbf{S}^T - \mathbf{J} \right) / (n + 1), \quad (5)$$

where **J** is an all-ones matrix and the superscript *T* denotes the transpose, respectively.

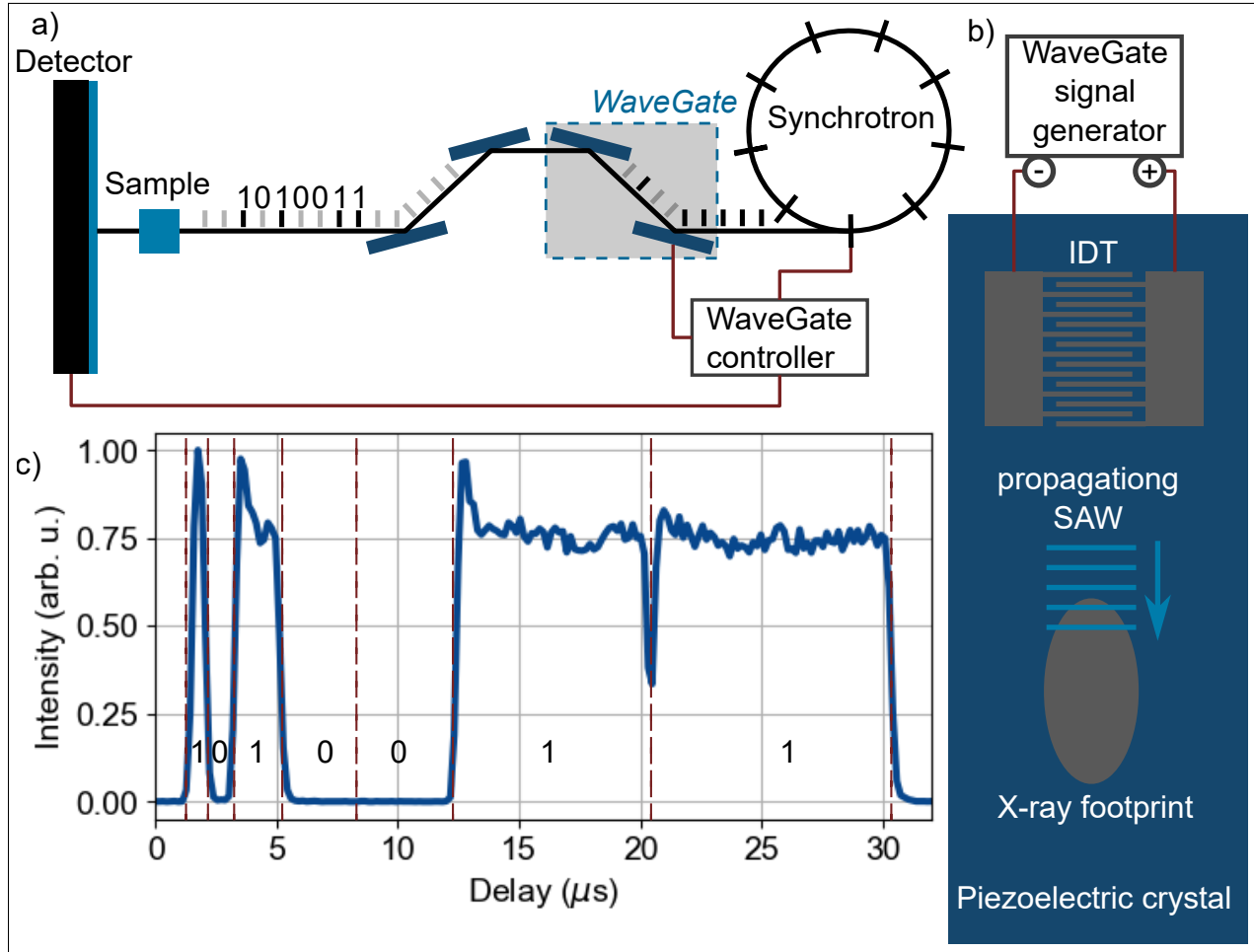


Figure 2: **Experimental technique:** a) General beamline setup for synchrotron-based experiments using the *WaveGate* pulse picker. X-ray pulses are emitted from a synchrotron storage ring and impinge on the *WaveGate* setup.<sup>17</sup> The subsequent two crystals compensate for the change in beam height introduced by the *WaveGate*. This stage was used in the experiment discussed in Section but not in the one in Section . b) Top view on the active crystal of the *WaveGate* pulse picker. The interdigitated transducer (IDT) is exposed to a RF signal which is converted into a surface acoustic wave (SAW) by the piezoelectric substrate. The SAW modulates the diffraction efficiency of a structural Bragg reflex, thus enabling the transmission or suppression of the incident x-ray pulses. The device is discussed in detail elsewhere.<sup>17</sup> c) Exemplary probe pulse sequence with 7 time windows of variable duration: 700 ns, 1000 ns, 2000 ns, 3000 ns, 4000 ns, 8000 ns, 10000 ns. The individual windows are separated by a red dashed line and contain the binary value of the matrix.

## Back-and-forth motion of a linear translation stage along the x-ray beam axis monitored by Debye-Scherrer diffraction

This first demonstration measurement was performed at the T-REXX endstation on beamline P14 at the PETRA III storage ring and the experimental setup is depicted in Figure 3 a). The general beamline layout with the installed *WaveGate* pulse picker was already discussed in the previous section . The x-ray beam with the modulated pulse sequences impinges a  $\text{Cr}_2\text{O}_3$  Eskolaite powder sandwiched between two Mylar foils. The sample was mounted on a linear translation stage that performed a repetitive back-and-forth motion along the x-ray beam axis  $\Delta D$ . The incident beam had a photon energy of 12.7 keV. It diffracted into several Debye-Scherrer rings that were captured by an area detector (Eiger 4M, Dectris). Figure 3 b) depicts a section of a typical detector image. The area around the (110) ring marked by the red square is magnified in Figure 3 c).

The synchronization and timing scheme that was implemented for this measurement is as follows. The  $n=7$  time windows had an equal duration of 5 ms with a duty cycle of 50%. Hence, a logical 1 is represented by a 2.5 ms x-ray pulse followed by a 2.5 ms dark period. A logical 0 is represented by a 5 ms dark period. The translation stage provided a trigger signal that was used to synchronize the probe pulse sequence generated by the *WaveGate*. After the 7-window sequence completed, the *WaveGate* blocked the incident x-ray beam from the storage ring. Images were recorded, synchronised to always start at the same stage position, with an overall exposure time of 100 ms.

Figure 3 b) displays a blurring<sup>23</sup> of the Debye-Scherrer rings that stems from the mechanical motion of the Eskolaite powder sample mounted on the translation stage. In the magnified area displayed in Figure 3 c) we recognize the temporal probe sequence 1010011 (right to left). This sequence corresponds to the third column of the **S**-matrix displayed in Equation 4 and the image represents measurement  $W_3$  according to the formalism laid out in Section . With the full set of images  $W_0$  to  $W_6$  we perform the inverse transformation  $R = S^{-1} \times W$  to find the position of the powder ring on the detector and thereby the

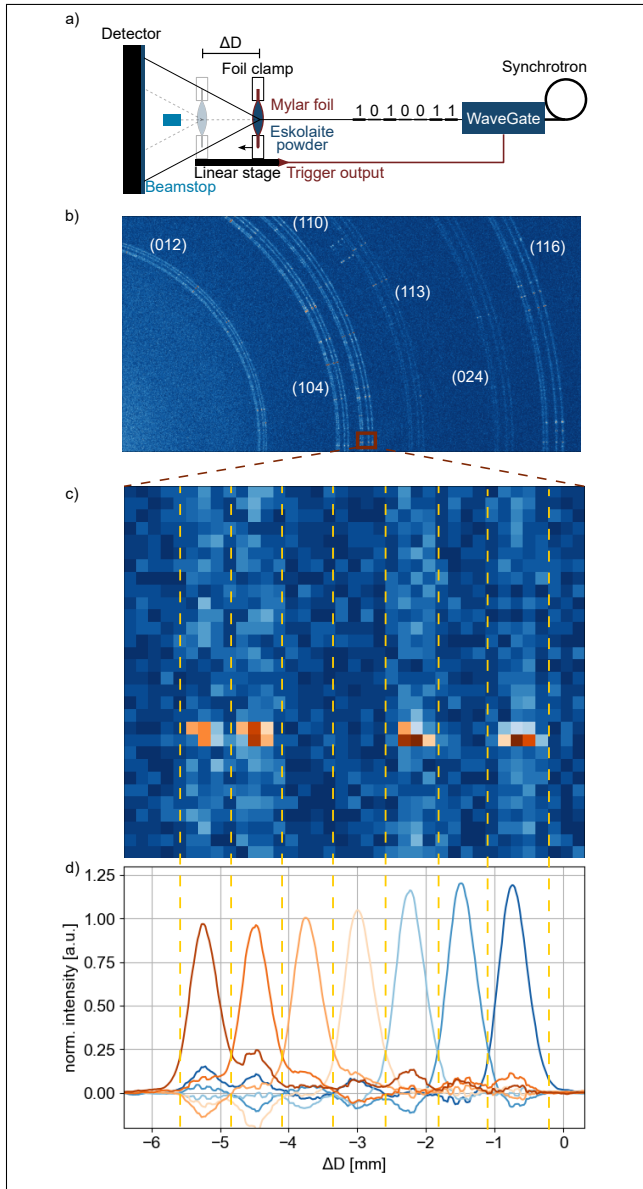


**Figure 3: First Advanced Timing Measurement:** a) Experimental Setup: an Eskolaite powder sample is attached to a linear stage that performs a periodic back-and-forth motion along the x-ray beam axis. Incident x-rays diffract from the sample in Debye-Scherrer rings with a radius depending on the transient position of the translation stage as the sample to detector distance was varied. The sample was probed with a probe sequence generated by the *WaveGate* pulse picker. b) Detector image depicting multiple Debye-Scherrer diffraction rings from the sample. The rings display a motion blur with a modulated intensity. c) Detailed view of the (110) Debye-Scherrer ring. The intensity modulation displays the inverted (from right to left) probe sequence 1010011. d) Transient stage position obtained after the inverse transform with the full dataset.

transient position of the translation stage in each time window  $t_n$ . The result is depicted in Figure 3 d), where early delay windows are coded in blue and later delays are coded in red.

By employing the inverse transformation we can determine the transient position of the stage even though the detector images are blurred due to the moving sample. The measured intensity at the different positions is reduced at later delays and we observe a smearing of the position in the corresponding traces. We suspect that the speed of the translation stage changes due to friction heating, which translates into slight position errors in the inverse transformation. This is a good example to point out the challenges and intricacies of this method. Because the probe pulses are distributed across many time windows, it is difficult to repeat a measurement of a specific delay. An error spreads over the entire delay axis and if in doubt, the full series must be repeated.

## **Micromechanical motion of a 500 nm thin membrane monitored by Laue diffraction**

We now discuss a second, more realistic demonstration measurement, where the transient response of the sample was not known in advance. The sample was a 500 nm thin SiN membrane which was coated with an amorphous 40 nm thin Pt film by magnetron sputtering. The experimental setup was very similar to the scheme depicted in Figure 2 a). We performed this experiment at beamline P23 at the PETRA III storage ring and a schematic is given in Figure 4 a). The sample was mounted in the direct beam diffracted from the second *WaveGate* crystal. The x-ray beam was moderately focused to a spot size of  $30 \mu\text{m} \times 160 \mu\text{m}$  by a set of Be compound refracting lenses located 30 m upstream from the sample position. We captured the (100) diffraction ring in Laue geometry with an area detector (Lambda 750k, XSpectrum). The distance between sample and detector was 1 m and the diffracted beam from the sample covered the entire detector area of  $28 \times 85 \text{ mm}^2$ . With the available detector area we captured only a small fraction of the total radiation diffracted from the sample.

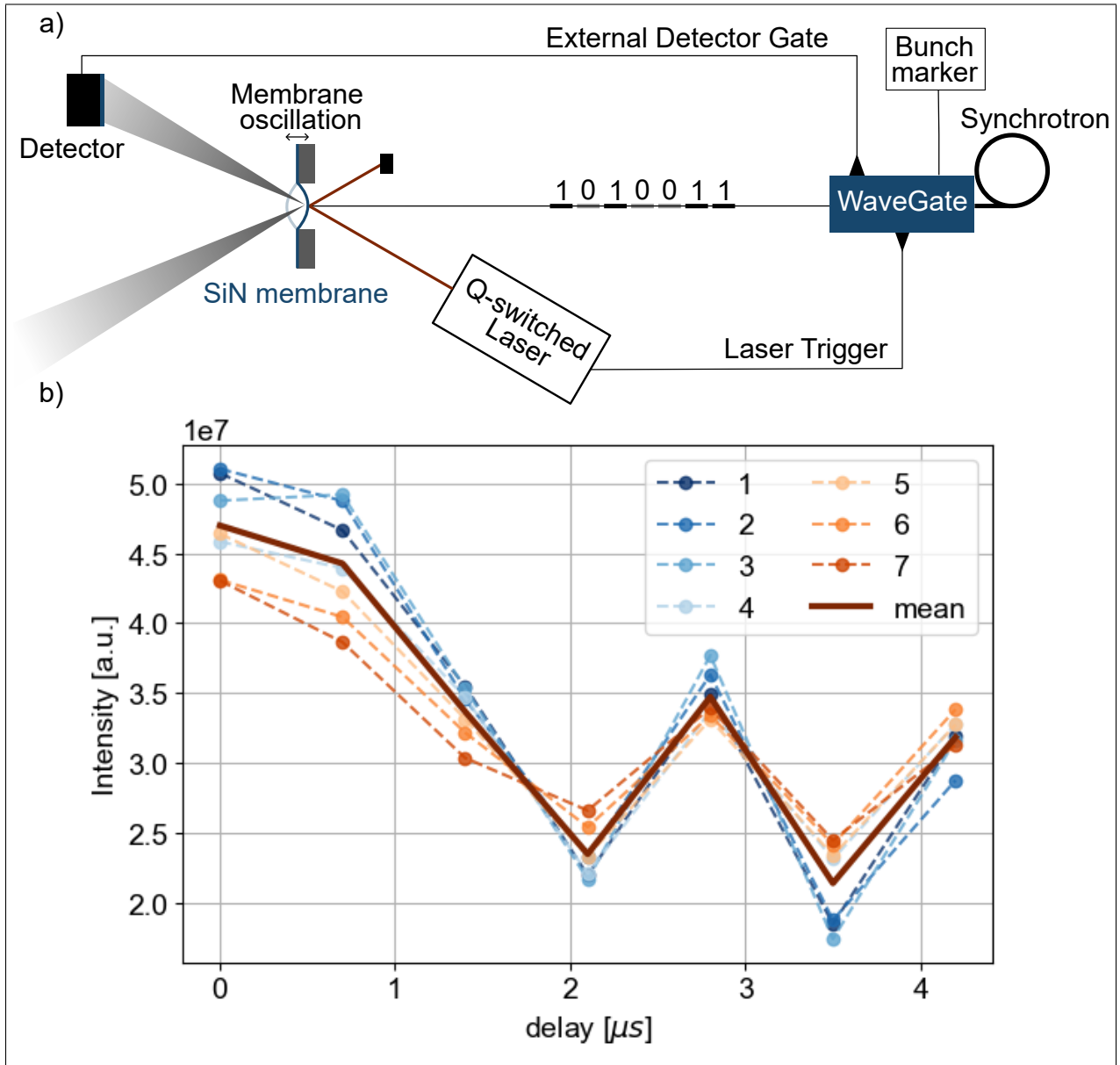


Figure 4: **Second Advanced Timing Measurement:** a) Experimental setup: The *WaveGate* pulse picker was synchronized to the bunchmarker signal from the storage ring and generated trigger signals for the excitation laser and area detector. The sample (SiN membrane with 40 nm Pt coating) was excited by 7 ns laser pulses with a wavelength of 1064 nm. The subsequent dynamics were probed by alternating sequences of probe pulses generated by the *WaveGate* pulse picker. Incident x-rays were diffracted in Debye-Scherrer rings of which only a small fraction were captured by the area detector. b) Transient sample dynamics obtained from the inverse transformation using all recorded probe sequences. Each sequence was recorded ten times (bullets, dashed) to demonstrate the reliability of the measurement. The average response is depicted in the red solid line.

To elicit a transient response, we exposed the sample to laser pulses with a duration of 7 ns, a wavelength of 1064 nm and a pulse energy of 1 mJ. The laser footprint at the sample position was almost circular, with a radius of 500  $\mu$ m. The sample was excited at a repetition rate of 1 kHz with an incident fluence of 40.7 mJ/cm<sup>2</sup>.

The storage ring operated in 40 bunch mode, *i.e.*, subsequent x-ray pulses were separated by a gap of 192 ns. By reducing the repetition rate of the experiment to the 1 kHz repetition frequency of the laser we reduce x-ray flux for the time-resolved experiment by a factor of 5200.<sup>24</sup> In addition, the largest fraction of the diffracted beam was not captured by the relatively small area detector. Hence, a pump-probe measurement was too insensitive to capture the laser-induced dynamics of the membrane. The experiment was therefore an ideal test for the advanced Hadamard timing scheme. Again, we used the  $7 \times 7$  **S**-matrix given in Equation 4, this time with a duration  $\delta t$  of the time windows of 700 ns. The *WaveGate* was synchronized to the bunchmarker signal. A trigger signal for the laser and an external gating signal for the area detector were generated by the *WaveGate* electronic hardware. The external gating was active for the total duration of the probe pulse sequence. We tuned the delay axis such that the first delay point  $t_0$  coincided with the arrival of the laser pump pulse at the sample. Therefore, no negative delay times were measured. For every probe pulse sequence we captured ten redundant images. Thus, we performed a total of 10 delay scans over a delay range of 4.2  $\mu$ s.

The transient sample response for the ten independent measurements was obtained through the inverse transform  $\mathbf{R} = \mathbf{S}^{-1} \times \mathbf{W}$ . Results are depicted in Figure 4 b) in the colored dashed lines. The dark red solid line shows the average of all measurements. We observe a continuous decay from the first to the last measurement, which indicates a laser-induced degradation of the sample. Otherwise, all ten measurements show a qualitatively identical temporal response. At this point we refrain from speculating about the underlying physical mechanism responsible for the observed dynamics. The only purpose of this measurement is to demonstrate the reliability of the advanced timing scheme.

## Summary and Conclusion

In conclusion we have demonstrated the implementation of advanced timing schemes for synchrotron-based time-resolved measurements by encoding of the incident x-ray beam. The new method employs probe sequences of probe pulses which are distributed along a delay axis according to a predefined rule derived from a Hadamard transform. By performing the inverse transform the transient response of a sample at each delay can be obtained. The main advantage of this timing scheme is its increased sensitivity and the increase photon flux during the measurement.

A prerequisite to employ the new timing scheme is the ability to generate alternating probe sequences with high accuracy and variability. Our solution to this challenge is the *WaveGate* pulse picker. It is a versatile device that integrates easily in different beamline environments and allows the generation of probe patterns at the beamline control interface.

We demonstrated the feasibility of our method with two exemplary measurements that were performed at different beamlines at the PETRA III storage ring at DESY, Hamburg.

## Acknowledgment

The T-REXX endstation and the development of the *WaveGate* pulse picker for encoding Hadamard sequences are supported by the Bundesministerium für Bildung und Forschung (Verbundforschungsprojekte 05K16GU1, 05K19GU1 & 05K22GU6).

Beamtime at T-REXX was provided by the T-REXX BAG at EMBL (MX862). We acknowledge DESY (Hamburg, Germany), a member of the Helmholtz Association HGF, for the provision of experimental facilities. Parts of this research were carried out at Petra III and we would like to thank Dr. Dmitry Novikov and Dr. Azat Khadiev for assistance in using Beamline P23. Beamtime was allocated for proposal I-20220569.

## Disclosures

The authors declare no conflicts of interest.

## Data availability

Data underlying the results presented in this paper are not publicly available at this time but may be obtained from the authors upon reasonable request.

## References

- (1) Shin, S. New era of synchrotron radiation: fourth-generation storage ring. *AAPPS Bulletin* **2021**, *31*, 1–16.
- (2) Chapman, H. N. Fourth-generation light sources. *IUCrJ* **2023**, *10*, 123–134.
- (3) Gaal, P.; Schick, D.; Herzog, M.; Bojahr, A.; Shayduk, R.; Goldshteyn, J.; Navirian, H. A.; Leitenberger, W.; Vrejoiu, I.; Khakhulin, D.; Wulff, M.; Bargheer, M. Time-domain sampling of x-ray pulses using an ultrafast sample response. *Applied Physics Letters* **2012**, *101*, 243106.
- (4) Enquist, H.; Navirian, H.; Nüske, R.; von Korff Schmising, C.; Jurgilaitis, A.; Herzog, M.; Bargheer, M.; Sondhauss, P.; Larsson, J. Subpicosecond hard x-ray streak camera using single-photon counting. *Opt. Lett.* **2010**, *35*, 3219–3221.
- (5) Klureza, M. A.; Pulnova, Y.; von Stetten, D.; Owen, R. L.; Beddard, G. S.; Pearson, A. R.; Yorke, B. A. In *Time-Resolved Methods in Structural Biology*; Moody, P., Kwon, H., Eds.; Methods in Enzymology; Academic Press, 2024; Vol. 709; pp 177–206.
- (6) Jo, Y.; Park, H.; Lee, S.; Kim, I. Spectral Hadamard microscopy with metasurface-based patterned illumination. *Nanophotonics* **2025**,

(7) Ēriks Kupčē; Freeman, R. Two-dimensional Hadamard spectroscopy. *Journal of Magnetic Resonance* **2003**, *162*, 300–310.

(8) Rousseau, G.; Blouin, A. Hadamard multiplexing in laser ultrasonics. *Opt. Express* **2012**, *20*, 25798–25816.

(9) Coufal, H.; Moller, U.; Schneider, S. Photoacoustic imaging using the Hadamard transform technique. *Appl. Opt.* **1982**, *21*, 116–120.

(10) Nelson, E. D.; Fredman, M. L. Hadamard Spectroscopy. *J. Opt. Soc. Am.* **1970**, *60*, 1664–1669.

(11) Beddard, G. *Applying Maths in the Chemical and Biomolecular Sciences: An Example Based Approach*; Oxford University Press, 2009.

(12) Beddard, G. S.; Yorke, B. A. Pump–Probe Spectroscopy Using the Hadamard Transform. *Applied Spectroscopy* **2016**, *70*, 1292–1299, PMID: 27340218.

(13) Cao, G.; Zhang, J.; Zhou, O.; Lu, J. Temporal multiplexing radiography for dynamic x-ray imaging. *Review of Scientific Instruments* **2009**, *80*, 093902.

(14) Yorke, B. A.; Beddard, G. S.; Owen, R. L.; Pearson, A. R. Time-resolved crystallography using the Hadamard transform. *Nature Methods* **2014**, *11*, 1131–1134.

(15) Sloane, N. J. A. In *Fourier, Hadamard, and Hilbert Transforms in Chemistry*; Marshall, A. G., Ed.; Springer US: Boston, MA, 1982; pp 45–67.

(16) Harwit, M.; Sloane, N. J. A. *Hadamard Transform Optics*; Academic Press: New York, 1979.

(17) Schmidt, D.; Hensel, D.; Petev, M. V.; Khosla, M.; Brede, M.; Vadilonga, S.; Gaal, P. WaveGate: a versatile tool for temporal shaping of synchrotron beams. *Optics Express* **2024**, *32*, 7473.

(18) Götz, A.; Taurel, E.; Pons, J.-L.; Meyer, J.; Chaize, J.-M.; Perez, M. TANGO Controls: A successful collaboration for open-source control systems. ICALEPCS'19: International Conference on Accelerator and Large Experimental Physics Control Systems. 2020.

(19) Dalesio, L. R.; Hill, J.; Kraimer, M. R.; Shen, G.; Clausen, M.; Veseli, S. EPICS: The Next Generation. ICALEPCS'19: International Conference on Accelerator and Large Experimental Physics Control Systems. 2020.

(20) Delgado, A.; Coutinho, T.; Guijarro, D.; Meyer, J.; Perez, M.; Pons, J. L.; Taurel, E. BLISS: The Beamline Instrumentation Support Software. ICALEPCS'19: International Conference on Accelerator and Large Experimental Physics Control Systems. 2020.

(21) Allan, D. B.; Caswell, T. A.; Campbell, S. I.; Rakitin, M. S.; Bettis, J.; Clausen, M.; Dalesio, L. R.; Hanwell, M. D.; Lynch, K.; Perry, S. L.; others BlueSky: A Python framework for experiment control and data acquisition. ICALEPCS'19: International Conference on Accelerator and Large Experimental Physics Control Systems. 2019.

(22) of Crystallography, I. U. *Acta Crystallographica Section A: Foundations and Advances*. *Acta Crystallographica Section A: Foundations and Advances* **2019**, *75*, 123–456.

(23) Harke, K. J.; Armstrong, M. R.; Martinez, D.; Lind, J.; Kumar, M. Quantifying motion blur by imaging shock front propagation with broadband and narrowband X-ray sources. *Scientific Reports* **2024**, *14*, 25580.

(24) Gaal, P.; Schmidt, D.; Khosla, M.; Richter, C.; Boesecke, P.; Novikov, D.; Schmidbauer, M.; Schwarzkopf, J. Self-stabilization of the equilibrium state in ferroelectric thin films. *Applied Surface Science* **2023**, *613*, 155891.